

## Numerical Solution of 2D Natural Convection in a Concentric Annulus with Solid-Liquid Phase Change

R. Avila<sup>1</sup> and F.J. Solorio<sup>1</sup>

**Abstract:** Heat transfer processes involving phase change either, solidification or melting, appear frequently in nature and in industrial applications. In this paper the convective patterns that arise from a 2D shear driven annular flow (without and with melting), are presented. The convective annular flow with radial gravity can be considered as a simplified model of the atmospheric flow in the terrestrial equatorial plane (bounded by the warm surface of the Earth and the cold tropopause). The governing equations have been numerically solved by the Spectral Element Method. The numerical results reported in this paper, for the cases without melting (at two different radius ratio  $\eta=r_i/r_o$ ) are in qualitative agreement with analytical results and experimental data obtained elsewhere for 2D annular electroconvection systems. For the cases with melting, the material between the two concentric circles (with radius ratio  $\eta=0.35$ ) is initially solid. The melting process takes place from the internal circle with temperature  $T_h$ , where  $T_h$  is greater than the melting temperature  $T_m$ . The heat transfer rate at the internal circle and the convective flow patterns have been obtained for the cases without shear and with shear. The Couette shear is induced by a constant rotation of the internal circle. As the phase change process takes place, three parameters of the system depend on the fluid layer depth: the Rayleigh number, the Reynolds number and the radius ratio of the annular fluid layer. We found that as the fluid layer depth increases, different flow patterns appear. We discuss the critical azimuthal mode number and its relationship with the Nusselt number.

**Keywords:** Natural convection, Concentric annulus, Melting

### 1 Introduction

Phase change processes (solid-liquid) frequently appear in nature and industrial applications. In nature, the melting and solidification processes are found in geophys-

---

<sup>1</sup> Departamento de Termofluidos, Facultad de Ingeniería, Universidad Nacional Autónoma de México, Mexico D.F. C.P. 04510. E-mail: ravila@servidor.unam.mx and fjsol@servidor.unam.mx

ical systems such as the growth of Earth's crust and the ice formation (or melting) in the Earth's polar regions. In industrial applications, phase change phenomena are present in the cast of pure metals and alloys, in mono-crystal growth techniques and in plastic extrusion manufacturing processes. It is well known that the mono-crystal growth industry and the cast of pure metals processes demand a strict quality control of the final product. The quality of the product strongly depends on the characteristics of the convective flow patterns which may transport impurities towards the region where the pure material is forming. In this paper the characteristics of the convective patterns in a Boussinesq fluid confined between two circles (annular thermal convection) are investigated.

In the first part of the paper, the convective flow patterns in 2D, annular regions without and with shear (circular Couette flow) in the absence of phase change, are presented. These calculations were performed to qualitatively compare the thermal convective patterns with the annular electroconvection patterns appearing in smectic-A liquid crystal thin films [Zahir, Deyirmenjian, Morris, and Bruyn (1998); Zahir, Deyirmenjian, and Morris (1999); Deyirmenjian, Zahir, and Morris (2005); Tsai, Zahir, Deyirmenjian, and Morris (2007)]. Even though the two systems share the same geometry and the same symmetry groups, the comparison is qualitative because the source of instability, the physical properties and the scales are very different. In the calculations, the three parameters governing the pattern formation (the radius ratio  $\eta = r_i/r_o$ , the Rayleigh number  $Ra$  and the Reynolds number  $Re$ ) have constant values.

In the second part of the paper, an additional parameter which governs the rate of melting of the initially solid annular region, the Stefan number  $St$ , is introduced. Notice that by inducing a melting process from the inner circle, the  $\eta$ ,  $Ra$  and  $Re$  parameters of the system are time dependent because the characteristic length is directly related to the position of the interface (melting front). Hence we have a dynamic process where the thermal convective modes are (i) appearing, (ii) disappearing, and (iii) interacting, as the parameters  $\eta$ ,  $Ra$  and  $Re$  change. To the best knowledge of the authors, research work in annular thermal convection with shear and melting, has not been previously reported.

The qualitative comparison performed in the first part of this research (without phase change and without Couette flow,  $Re=0$ ) has been based on the theoretical study carried out by Langford and Rusu (1998). They investigated the stationary and spatio-temporal flow patterns taking place in a region between two concentric circles in a plane (two dimensional annular convection). They showed, by applying the model independent Equivariant Bifurcation Theory, that the type of flow patterns that can be observed in an annular region, are mainly determined by purely mathematical properties such as geometry and symmetry groups. They found that

the loss of stability (bifurcation) of the basic motionless condition leads to a convective motion which can be described as a chain of pairs of clockwise/counterclockwise vortices around the annulus. The number of such pairs (the mode number  $m$ ) depends on both parameters  $\eta$  and  $Ra$ . Langford and Rusu (1998) analyzed those aspects of convective pattern formation that characterize two phenomena which occur at very different spatial scales: (1) the atmospheric thermal convective motion in the terrestrial equatorial troposphere, and (2) the annular electroconvection in smectic- $A$  liquid crystal thin films [Langford and Rusu (1998)]. For the atmospheric case, the flow patterns appear due to the gravity force vector directed radially towards the centre of the Earth and the temperature difference between the warm surface of our planet and the cold tropopause. In the second case the instability source is a radial electrical force in the suspended annular smectic liquid crystal film. The development and use of a simplified two dimensional Boussinesq model (such as the one developed in this investigation) to predict the atmospheric air convective patterns in the terrestrial equatorial plane, is fully justified, from the physical point of view. Recent observations have revealed the presence of large scale waves in the equatorial troposphere [Tsuda, Murayama, Wiryosumarto, Harijono, and Kato (1994a); Tsuda, Murayama, Wiryosumarto, Harijono, and Kato (1994b)]. It has been established that in the equatorial region (where the background mean winds are much weaker than the mean winds at middle latitudes), convection in the troposphere is the main excitation source of large scale waves. Measurements in the equatorial troposphere have also identified upward and downward large scale energy propagating waves. The analysis of the thermal convection through the use of a two dimensional Boussinesq model, may lead to get a more clear understanding of the atmospheric phenomena that appear in the equatorial plane.

Regarding the cases without phase change but with rotation of the inner circle, it should be mentioned that theoretical, numerical and experimental research on pattern formation in annular electroconvection, with imposed shear at the internal circle, have been carried out in the weakly nonlinear regime [Zahir, Deyirmenjjan, Morris, and Bruyn (1998); Zahir, Deyirmenjjan, and Morris (1999); Deyirmenjjan, Zahir, and Morris (2005); Tsai, Zahir, Deyirmenjjan, and Morris (2007)]. It has been reported that the basic mechanisms of the electrohydrodynamic convection instability in nematic liquid crystals is analogous to the Rayleigh-Bénard convection with radial driving constant gravity force. The linear theory of the annular convective instability is well established including the case of an annular geometry with imposed shear [Zahir, Deyirmenjjan, and Morris (1999)]. In the research on pattern formation in annulus with circular Couette flow, it has been identified the presence of stationary and traveling patterns, as well as localized structures.

In this investigation it has been found that in the absence of Couette shear the bi-

furcation from the heat diffusion state to the convective condition, results in a stationary flow pattern consisting on counter-rotating pairs of vortices lying around the circumference of the annulus. Each pair of vortices has reflection symmetry and the overall pattern is spatially periodic and 1D in the azimuthal direction, which is in agreement with the theoretical findings and experimental data obtained in electroconvective phenomena [Zahir, Deyirmenjjan, and Morris (1999); Zahir, Deyirmenjjan, and Morris (2001)]. It has been also found that when Couette flow is applied at the internal circle, an azimuthally traveling pattern is present, and the azimuthal mode is reduced, which is also in agreement with the electroconvection experiments. It has been reported that when the annular flow is sheared, the reflection symmetry of the base state is not present. And when the flow is driven, the pattern breaks the azimuthal symmetry, hence the pattern is free to travel azimuthally in the direction of the mean flow [Zahir, Deyirmenjjan, and Morris (2001)]. Zahir et al. (1999) calculated the neutral stability boundary as a function of the radius ratio  $\eta$  and the Reynolds number  $Re$  of the shear flow. In the research that we report in this paper, numerical simulations were carried out aimed to study the influence of a shear Couette flow on the natural convection and shape of the interface in a melting process that takes place in an annular region confined between two concentric circles. The critical control parameters  $Ra$ ,  $\eta$  and  $Re$ , and the critical azimuthal mode number  $m_c$  have been identified. It has been found that the Couette flow suppresses the onset of the convection (similar to the electroconvection findings i.e.  $Ra_c(\eta, Re) > Ra_c(\eta, 0)$ ). It can be concluded that the numerical simulations reproduce qualitatively well the theoretical, numerical and experimental results obtained in an electroconvection system, consequently, it is possible to mention that the complex dynamical phenomena appearing in the melting process of a 2D concentric annular solid, are properly evaluated. The paper is organized as follows: In Sec. 2 the physical and mathematical models are presented. In Sec. 3 the numerical algorithm is briefly described. In Sec. 4 the numerical results are shown. In Sec. 5 the concluding remarks are presented.

## 2 Mathematical model

We have investigated the natural convection of an incompressible fluid confined in an annular region bounded by two concentric circles with radius  $r_i$  (internal) and  $r_o$  (external), see Fig. 1. The internal circle is at a temperature  $T_h$  whereas the external circle is at a temperature  $T_c$ , where  $T_h > T_c$ . The convective flow patterns appear due to the constant gravity force vector directed radially towards the centre of the circles, and the temperature difference. It is assumed that the physical properties (except the density) of the fluid remain constant. The density variation will be only considered in the buoyancy term of the momentum equation (Boussinesq approx-

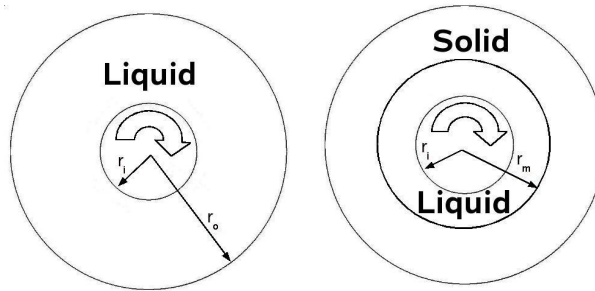


Figure 1: Natural convection in a concentric annular region. Left: With no melting; the liquid is confined in the annular region bounded by two concentric circles with radii  $r_i$  and  $r_o$ . Right: With melting; initially the solid phase occupies the whole annular region, The melting process of the solid annulus is from the internal circle. The arrows mean clockwise rotation of the internal circle.

imation). To nondimensionalize the equations we use the gap width  $d=r_o - r_i$ , the diffusive thermal time  $t_d=d^2/\alpha$ , where  $\alpha$  is the thermal diffusivity, and the temperature difference between the temperature of the inner circle and the temperature of the outer circle:  $\Delta T = T_h - T_c$ . The temperatures in the liquid phase and in the solid phase have been nondimensionalized as:

$$\Theta_l = \frac{T_l - T_c}{T_h - T_c} = \frac{T_l - T_c}{\Delta T} \quad (1)$$

and

$$\Theta_s = \frac{T_s - T_c}{T_h - T_c} = \frac{T_s - T_c}{\Delta T}, \quad (2)$$

respectively. The nondimensional temperature of the interface is written as

$$\Theta_m = \frac{T_m - T_c}{T_h - T_c} = \frac{T_m - T_c}{\Delta T} \quad (3)$$

It may be observed that the range of the temperatures  $\Theta_l$  and  $\Theta_s$  is

$$0 \leq \Theta_s \leq \Theta_m \quad \text{and} \quad \Theta_m \leq \Theta_l \leq 1 \quad (4)$$

Assuming that the thermal diffusivities and the thermal conductivities in the liquid and in the solid are the same i.e.  $\alpha_l=\alpha_s$  and  $\kappa_l=\kappa_s$ , the nondimensional flow governing equations are written as

Continuity equation

$$\nabla \cdot \mathbf{u} = 0 \quad (5)$$

Momentum equation

$$\frac{\partial \mathbf{u}}{\partial t} + \mathbf{u} \cdot \nabla \mathbf{u} = -\nabla p + Pr \nabla^2 \mathbf{u} + Ra Pr \Theta_l \quad (6)$$

Energy equation

$$\frac{\partial \Theta_l}{\partial t} + \mathbf{u} \cdot \nabla \Theta_l = \nabla^2 \Theta_l \quad (7)$$

where  $Pr$  is the Prandtl number defined as  $Pr = \nu/\alpha$ , ( $\nu$  is the kinematic viscosity). The parameter  $Ra$  is the Rayleigh number. It is well known that if the density of the fluid varies linearly with the temperature, the Rayleigh number is commonly defined as

$$Ra = \frac{\beta g \Delta T d^3}{\nu \alpha} \quad (8)$$

where  $\beta$  is the thermal expansion coefficient. The radial gravity vector acts towards the centre of the circles; it is defined as

$$\mathbf{g} = -g \cdot \mathbf{e}_r \quad (9)$$

where  $\mathbf{e}_r$  is the unit vector along the radial direction, and  $g$  is a gravity constant. To study the convective pattern formation in a melting process, we also need to solve the heat equation that governs the temperature distribution in the solid phase. However for the cases with phase change considered in this investigation, it is assumed that the external circle remains at the same temperature than the melting point. Therefore there is no heat transfer in the solid phase and the heat equation for the solid was not solved. Additionally, the heat balance equation governing the rate of displacement of the interface must be considered. As the heat transfer through the solid phase has been neglected, the heat balance equation is written as

$$St v = -\nabla \Theta_l \cdot \mathbf{n} \quad (10)$$

where  $v$  is the nondimensional velocity of the interface in the direction of the outward normal unit vector  $\mathbf{n}$  and the parameter  $St$  is the Stefan number defined as

$$St = \frac{L_q}{c_p \Delta T}, \quad (11)$$

$L_q$  is the latent heat, and  $c_p$  is the specific heat. In the numerical simulations with phase change, we assume that initially the solid phase occupies the whole annular region. At the initial time, the temperature of the whole system is at the temperature  $\Theta_s=0$  which is equal to the cold temperature imposed at the outer boundary located at the external radius  $R_o = 1/(1 - \eta)$ , where  $\eta$  is the radius ratio, which is defined for the non-melting cases as  $\eta = r_i/r_o = 0.35$ . The phase change temperature is  $\Theta_m=0$  (the melting temperature is equal the temperature of the outer cold boundary), hence there is no heat transfer in the solid annulus. At a certain time, the temperature of the internal circle (at  $R_i=\eta/(1 - \eta)$ ) is raised and maintained at a temperature  $\Theta_h=1$ , while the temperature at the outer circle is maintained at the initial temperature  $\Theta_c=0$ , such that  $\Theta_h > \Theta_m = \Theta_c$ . The thermal boundary conditions lead to a melting process of the solid annulus from the internal surface, see Fig. 1. We assume no slip boundary conditions for the fluid on both circles, and for the cases with phase change, the no slip boundary condition is also assumed at the interface. The internal circle may have rotation, the constant rotation vector has only the component normal to the plane where the circles are defined ( $\vec{\Omega} = \Omega_3 \vec{i}_3$ ). The working fluid is water whose density is determined by the following fourth order polynomial [Inaba and Fukuda (1984)].

$$\rho = \rho_o + bT + cT^2 + dT^3 + eT^4 \tag{12}$$

where the coefficients have the following values (see Inaba and Fukuda (1984)):

$$b = 0.0673 \text{ kg}/(\text{m}^3 \text{ } ^\circ\text{C}), \quad c = -0.0089 \text{ kg}/(\text{m}^3 \text{ } ^\circ\text{C}^2) \tag{13}$$

$$d = 8.784 \times 10^{-5} \text{ kg}/(\text{m}^3 \text{ } ^\circ\text{C}^3), \quad e = -6.621 \times 10^{-7} \text{ kg}/(\text{m}^3 \text{ } ^\circ\text{C}^4), \tag{14}$$

the dimensional temperature  $T$  is given in ( $^\circ\text{C}$ ) and  $\rho$  in ( $\text{kg}/\text{m}^3$ ). Notice that the density has a maximum at  $T = 4^\circ\text{C}$ , hence in the cases with melting, a region with density inversion is present close to the interface (from  $T = 4^\circ\text{C}$  to  $T = 0^\circ\text{C}$ ). The nondimensional expression for the density (see Eq. (12)) is written as

$$\frac{\rho - \rho_o}{\rho_o} = \hat{b}\Delta T\Theta_l + \hat{c}(\Delta T\Theta_l)^2 + \hat{d}(\Delta T\Theta_l)^3 + \hat{e}(\Delta T\Theta_l)^4 \tag{15}$$

where:  $\hat{b} = b/\rho_o \text{ } 1/^\circ\text{C}$ ,  $\hat{c} = c/\rho_o \text{ } 1/^\circ\text{C}^2$ ,  $\hat{d} = d/\rho_o \text{ } 1/^\circ\text{C}^3$  and  $\hat{e} = e/\rho_o \text{ } 1/^\circ\text{C}^4$ . It should be mentioned that if the fourth order polynomial for the density is used, the buoyancy term in Eq. (6) may be written in a more complicated way such as

$$Pr(\hat{R}a_1\Theta_l + \hat{R}a_2\Theta_l^2 + \hat{R}a_3\Theta_l^3 + \hat{R}a_4\Theta_l^4) \tag{16}$$

where

$$\hat{R}a_1 = Ra = \frac{\hat{b}\Delta Tgd^3}{\nu\alpha}, \quad \hat{R}a_2 = \frac{\hat{c}\Delta T^2gd^3}{\nu\alpha}, \quad \hat{R}a_3 = \frac{\hat{d}\Delta T^3gd^3}{\nu\alpha}, \quad \hat{R}a_4 = \frac{\hat{e}\Delta T^4gd^3}{\nu\alpha} \tag{17}$$

Even though the values of the parameters  $\hat{c}$ ,  $\hat{d}$  and  $\hat{e}$  are small with respect to the value of the coefficient of the linear term  $\hat{b}$  (and hence the values of the Rayleigh numbers  $\hat{Ra}_2$ ,  $\hat{Ra}_3$  and  $\hat{Ra}_4$  are small with respect to the value of  $Ra$ ), they have been included in the calculations in order to take into account the inversion layer between  $0^\circ\text{C} < T < 4^\circ\text{C}$  and the non-linear variation of the density with the temperature.

Rotation of the inner circle about the axis located at the centre of the concentric circles leads to a Couette shear. To characterize the strength of the shear we use a Reynolds number defined as

$$Re = \frac{\Omega_3 r_i d}{\nu}, \quad (18)$$

the nondimensional expression of the rotation rate is  $\Omega^* = \Omega_3 t_d$ , and the nondimensional period is written as  $P = 2\pi/\Omega^*$ . As it was established,  $d$  for the non-melting cases is defined as  $d = r_o - r_i$ , whereas for the melting cases it is defined as  $d = r_m(t) - r_i$ , where  $r_m(t)$  is the radial position of the interface (at  $t = 0$ ,  $r_m(t = 0) = r_i$ ). The radius ratio with melting is defined as  $\eta_I = r_i/r_m(t)$ . Notice that as the melting process takes place, the position of the melting front  $r_m(t)$  is continuously changing, then the governing parameters  $Ra$ ,  $Re$  and  $\eta_I$  are time dependent.

### 3 The Spectral Element Method

The set of Eqs. (5)-(7) and (10) has been solved by using the Spectral Element Method (SEM) [Patera (1984); Rønquist and Patera (1987); Rønquist (1988); Karniadakis and Sherwin (1999)]. This methodology is a special case of the method of weighted residuals which leads to the Bubnov-Galerkin formulation (the expansion functions used to approximate the dependent variables, are the same as the weight functions). Using the SEM the computational domain is subdivided into large non-overlapping, quadrilateral (structured mesh), isoparametric macro-elemental regions ( $h$ -element size). Inside them, high order piecewise polynomial expansions ( $p$ -polynomial order) are defined. The SEM uses a polynomial nodal expansion based on Lagrange polynomials, which are associated with a set of nodal points that are located at the zeros of the Gauss-Lobatto-Legendre polynomials. The numerical quadrature is performed using a Gauss-Lobatto-Legendre quadrature rule, which corresponds to the same choice of the nodal points. The pressure field is calculated by using Gauss-Legendre points whereas the velocity field is solved by using Gauss-Lobatto-Legendre points (staggered grid approach). In the simulations that we present in this paper, the computational domain, corresponding to the union of the two phases, is a fixed domain. The liquid and solid phases are treated as time dependent domains separated by a moving interface. For moving interface

problems there are two basic methodologies to model the motion of the interface: moving-grid and fixed-grid methods. In the moving-grid approach, the interface is modeled as the boundary of a moving surface-fitted grid. This approach leads to a proper treatment of the interface, however in fluid flow problems with melting, the motion of the interface may conduct to a severe deformation of the mesh. In the second method, which is based on fixed grids, the moving interface is not explicitly tracked, but rather captured via a characteristic function [Mai-Duy, Mai-Cao, and Tran-Cong (2007); Mai-Cao and Tran-Cong (2008)]. The algorithm of moving interface used in this paper belongs to moving-grid methods. The algorithm is based on an interface local transformation-convective correction technique, together with a consistent interface flux evaluation [Rønquist and Patera (1987)]. A time dependent moving mesh technique has been implemented, in which the temperature distribution in each phase, is separately solved on fixed grids at every time step. In order to correct for dynamic domains a convective term is included in the energy equation of each phase. The new interface position is calculated by using Eq. (10). The shape of the interface and the geometry of the mesh are updated as shown by Rønquist and Patera (1987). After performing several tests in order to reach the mesh independence, it was decided to discretize the computational domain by using 150 spectral elements. For the cases without melting, the liquid domain in the concentric annulus was discretized by 30 macro-elements along the azimuthal direction and 5 macro-elements along the radius. In the melting cases, the mesh for the liquid phase was defined by 120 macro-elements (30 macro-elements along the azimuthal direction and 4 macro-elements along the radial direction). The mesh for the solid phase was defined by 30 macro-elements in the azimuthal direction and 1 set of macro-elements along the radial direction. The polynomial order of the expansion functions within each macro-element, was fixed to  $p = 9$ , along each direction. Using the SEM for the simulation of melting processes, both phases must always be present. In the simulations of this paper, the initial liquid phase was confined to a very thin annular region ( $[r_m(t = 0) - r_i] \rightarrow 0$ ). Therefore it is a good approximation to assume that at the beginning of the melting process, the solid phase occupies almost the whole annular region ( $r_o - r_i$ ). As the melting process takes place, the interface changes its position and morphology, and the liquid phase occupies more space within the annulus. Details of the numerical algorithm for the solution of the fluid equations and the algorithm used to calculate the displacement of the interface are reported by Rønquist(1988), Karniadakis and Sherwin(1999) and Rønquist and Patera (1987).

**4 Results**

Firstly we present the numerical simulations for the cases without melting. These are qualitatively compared with the analytical results and experimental data obtained in electroconvection systems [Zahir, Deyirmenjjan, Morris, and Bruyn (1998); Zahir, Deyirmenjjan, and Morris (1999); Deyirmenjjan, Zahir, and Morris (2005); Tsai, Zahir, Deyirmenjjan, and Morris (2007)]. Secondly, the numerical simulation of natural convection for the cases with melting is presented.

**4.1 Heat transfer in a concentric annulus with no phase change**

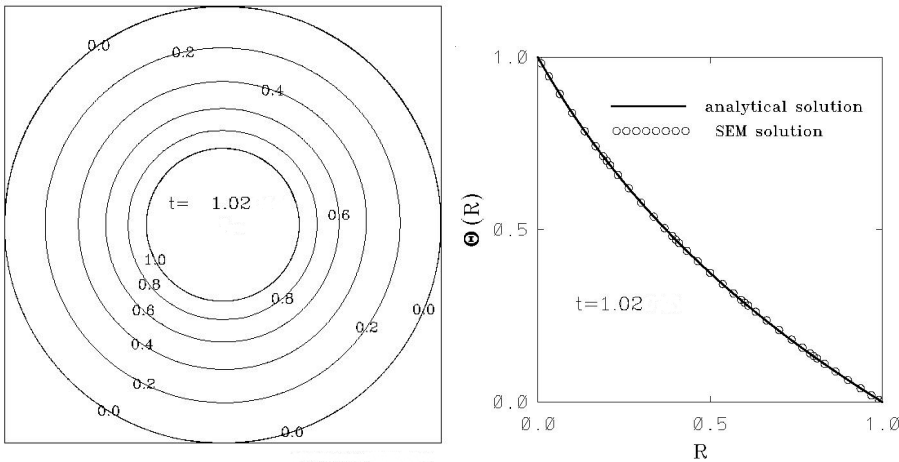


Figure 2: Steady state temperature distribution in a concentric annulus with no melting ( $t=1.02$ ). Subcritical regime (without convection). Left: Isothermal lines, the temperature increment between isotherms is  $\Delta\Theta=0.2$ . Right: Radial temperature distribution.  $Ra=1790$ ,  $\eta=0.35$ ,  $Re=0$ . Continuous line: Analytical solution Eq. (19). Symbols: SEM solution.

**4.1.1 Aspect ratio  $\eta=0.35$ , with no shearing ( $Re=0$ ) and subcritical conditions ( $Ra < Ra_c$ )**

The subcritical conditions lead to a diffusive one-dimensional heat transfer problem (basic flow without motion). It has been previously reported that the axisymmetric conductive regime becomes unstable to a flow pattern with an azimuthal wavenumber  $m=3$  at  $Ra_c=1799$  [Net, Alonso, and Sánchez (2003)]. The  $Ra$  number for this case was fixed at  $Ra=1790$ .

The analytical solution for the temperature distribution is

$$\Theta(R) = \frac{\ln [R + \eta (1 - R)]}{\ln (\eta)} \tag{19}$$

where  $R$  is the nondimensional radius defined as  $R=(r - r_i)/(r_o - r_i)$ . Fig. 2 shows the steady state isothermal lines, obtained by the SEM for a radius ratio  $\eta=0.35$ . It is observed that the isothermals are concentric circles due to the one dimensional heat conduction regime. Fig. 2 also shows the radial distribution of the temperature. As it is seen, the analytical solution and the results provided by the SEM are in full agreement.

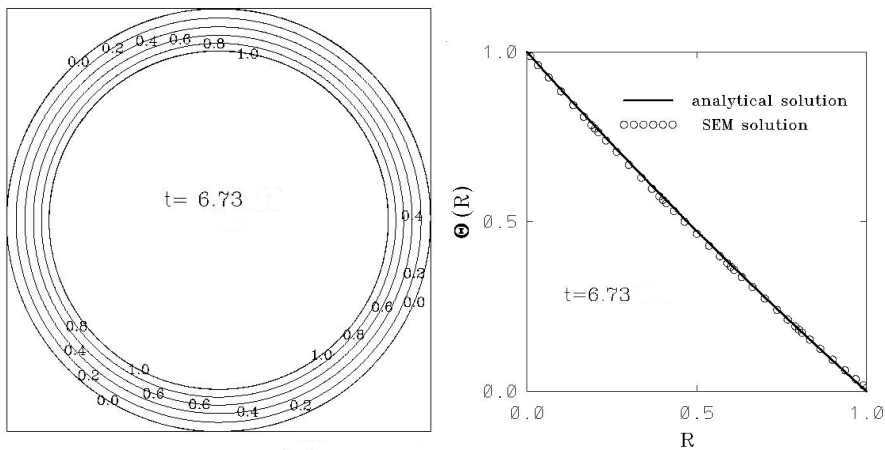


Figure 3: Steady state temperature distribution in a concentric annulus with no melting ( $t=6.73$ ). Subcritical regime (without convection). Left: Isothermal lines, the temperature increment between isotherms is  $\Delta\Theta=0.2$ . Right: Radial temperature distribution.  $Ra=450$ ,  $\eta=0.8$ ,  $Re=0$ . Continuous line: Analytical solution Eq. (19). Symbols: SEM solution.

4.1.2 Aspect ratio  $\eta=0.8$ , with no shearing ( $Re=0$ ) and subcritical conditions ( $Ra < Ra_c$ )

Fig. 3 shows the steady state isothermal lines obtained by the SEM for  $Ra=450$ . It is shown that the isothermals are again concentric circles due to the one dimensional conductive regime. The radial temperature distribution is also shown. The comparison between the analytical solution and the results provided by the SEM is also in full agreement.

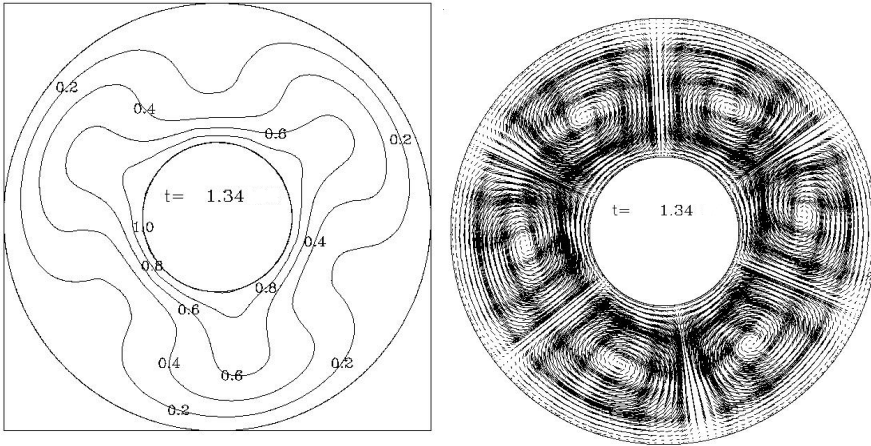


Figure 4: Steady state natural convection in a concentric annulus with no melting ( $t=1.34$ ). Supercritical regime. Left: SEM Isothermal lines, the temperature increment between isotherms is  $\Delta\Theta=0.2$ . Right: SEM velocity field.  $Ra=2000$ ,  $\eta=0.35$ ,  $Re=0$ . Critical mode number  $m_c=3$ .

#### 4.1.3 Aspect ratio $\eta=0.35$ , with no shearing ( $Re=0$ ), supercritical conditions ( $Ra=2000$ )

Fig. 4 shows the steady state isothermals obtained by the SEM. It is also shown the velocity vectors of the convective cells. It is seen that the SEM provides a convective mode  $m=3$ , which is in agreement with the predictions performed by Net et al. (2003). However Sahir et al. (1999) found in an electrically driven convection system without rotation, that for a radius ratio  $\eta=0.35$ , the critical mode number, evaluated by nonlocal stability analysis, is  $m_c=4$ , which is not in agreement with the pattern shown in Fig. 4. However it is observed that in the absence of shear, the convective flow consists of a stationary, azimuthally one-dimensional pattern of symmetric, counter-rotating vortex pairs, each pair of vortices has reflection symmetry, which is in full agreement with the results reported by Sahir et al. (1999).

#### 4.1.4 Aspect ratio $\eta=0.8$ , with no shearing ( $Re=0$ ), supercritical conditions ( $Ra=2240$ )

Fig. 5 shows the steady state isothermals obtained by the SEM. It is also shown the velocity vectors of the convective cells. It can be observed that the numerical solution provides a convective mode number  $m=15$ , which is not in agreement with the critical azimuthal mode number without shear  $m_c=18$ , reported by Sahir et al. (1999). Again in the absence of shear, the convective flow pattern is station-

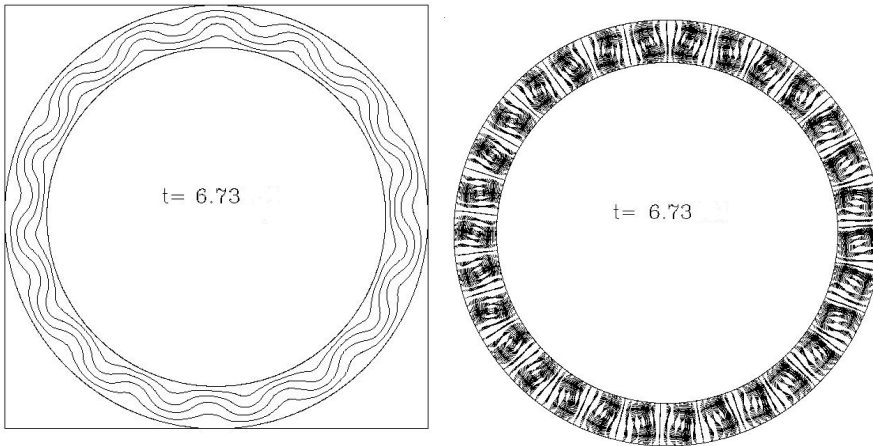


Figure 5: Steady state natural convection in a concentric annulus with no melting ( $t=6.73$ ). Supercritical regime. Left: SEM Isothermal lines, the temperature increment between isotherms is  $\Delta\Theta=0.2$ . Right: SEM velocity field.  $Ra=2240$ ,  $\eta=0.8$ ,  $Re=0$ . Critical mode number  $m_c=15$ .

ary with counter-rotating vortex pairs. Therefore, the comparison between thermal convection and electroconvection must be only considered as qualitative.

4.1.5 Aspect ratio  $\eta=0.35$ , with shear ( $P=0.02$ ), supercritical conditions ( $Ra = 7000$ )

This case shows the effect of a shear (applied by the clockwise rotation of the inner circle at a rate  $\Omega^*=325.7$ ,  $Re=13$ ), on the supercritical convective flow pattern. First of all it should be mentioned that due to the stabilizing effect of the shear on the convective onset ( $Ra_c$  increases with  $Re$ , indicating a suppression of thermal convection), it was necessary to increase the  $Ra$  number to  $Ra=7000$ , to have the convective onset. Fig. 6 shows the isothermal lines and the velocity field obtained by the SEM at four different times. It is observed that the effect of a circular Couette shear on the radially driven thermal convection is to promote the presence of a net mean flow in the azimuthal direction. Due to the shearing we do not obtain a chain of counter-rotating vortex pairs, but a big traveling vortex instead (i. e. the Couette flow reduces the azimuthal mode as was reported by Sahir et al. (1999)). The reduced critical wavenumber  $m_c$  that we obtained for this case ( $Re=13$ ), can not be compared even qualitatively with previous investigations. We also reproduce the results obtained by Sahir et al. in the sense that the traveling pattern appears as a meandering wave. It can be seen that when a rotation rate with period  $P=0.02$

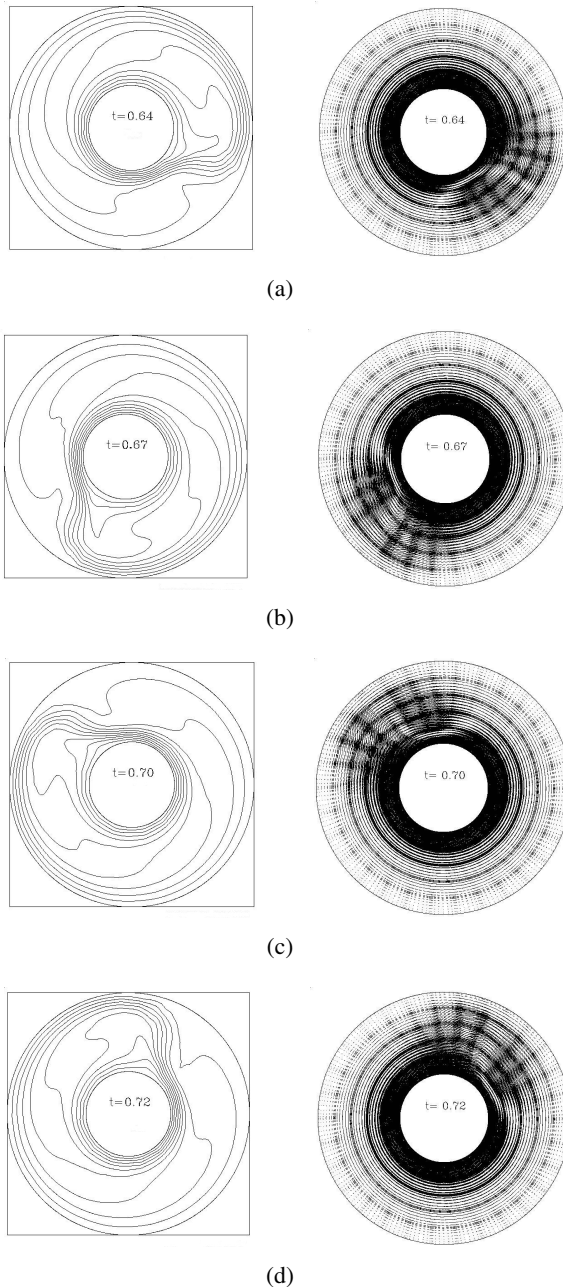


Figure 6: Non-steady natural convection in a concentric annulus with no melting. Periodic traveling pattern in a supercritical regime. Left: SEM Isothermal lines, the temperature increment between isotherms is  $\Delta\Theta=0.1$ . Right: SEM velocity field.  $Ra=7000$ ,  $\eta=0.35$ ,  $Re=13$ . Nondimensional period  $P=0.02$ .

is applied, the flow pattern is steadily periodic (independent of initial conditions). Our results indicate that the critical mode travels in the same sense as the inner circle.

**4.2 Heat transfer in concentric circles, with phase change  $St=3.9$**

In all the cases with phase change it is assumed that at time  $t=0$ , the annular region is occupied by the solid phase at a temperature  $\Theta_s=\Theta_m$ . At a certain instant the temperature of the inner circle is raised at a temperature  $\Theta_h$ , whereas the outer circle remains at a temperature  $\Theta_c=\Theta_m$ , therefore there is no heat transfer in the solid annulus.

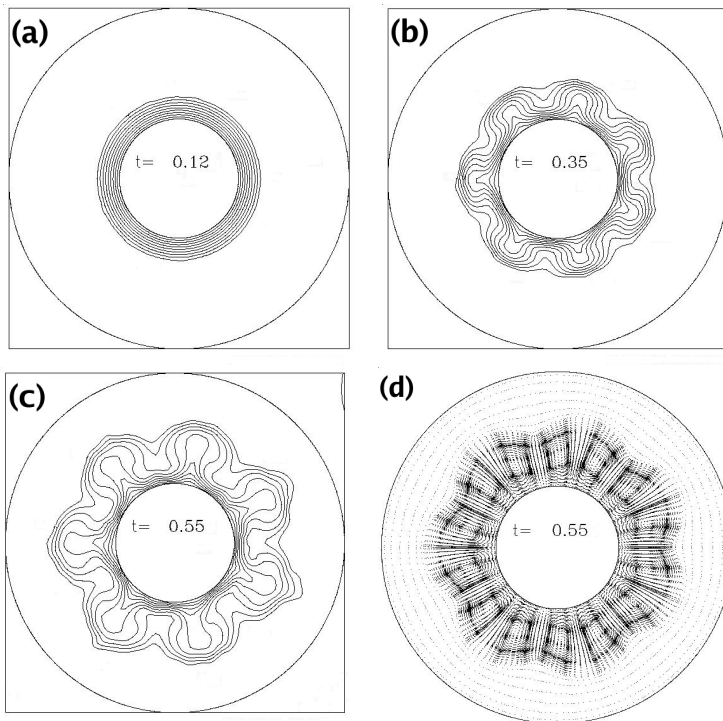


Figure 7: Non-steady natural convection in a concentric annulus with melting  $St=3.9$ .  $Ra$  and  $\eta_I$  are function of time. With no shearing  $Re=0$ . (a) Isothermal lines before convective onset  $t=0.12$ , (b) isothermal lines at convective onset  $t=0.35$ , (c) isothermal lines at  $t=0.55$ , and (d) velocity field at  $t=0.55$ . Critical mode number  $m_c=7$ . The temperature increment between isotherms is  $\Delta\Theta=0.1$ .

4.2.1 Melting of an initially solid annular region with radius ratio  $\eta=0.35$ , and with no shearing ( $Re=0$ )

Fig. 7 shows the isothermals at subsequent times. Notice that as the melting process takes place, the  $Ra$  number and the radius ratio  $\eta_I$  are time dependent.

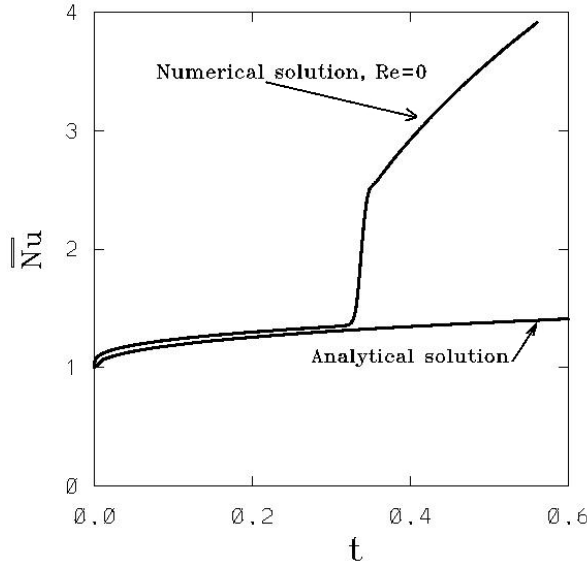


Figure 8: Average Nusselt number at the internal circle. With melting process,  $St=3.9$ . With no shearing  $Re=0$ .  $Ra$  and  $\eta_I$  are time dependent. Analytical solution Eq. (20).

It can be observed that once the critical conditions are reached, the convective patterns suddenly appear with an azimuthal mode number  $m_c=7$  (see Fig. 7 (d)). It can be seen that due to the interface deformation by the convective cells, the critical mode number  $m_c$ , does not change as the melting continues. The numerical simulation finishes when the deformation of the interface is severe and the Gauss-Lobatto-Legendre points overlap, hence a remeshing process is required. This is one of the drawbacks of the mesh based methods such as the SEM. In order to overcome this difficulty we propose to carry out in the future numerical simulations by using the numerical technique known as Meshless Local Petrov-Galerkin method. Meshless methods rely only on a group of arbitrarily distributed particles in the computational domain. The meshless methods not only avoid the generation of a numerical grid but also describe more accurately irregular geometries such as the shape of the interface in melting processes with natural convection [Lin and

Atluri (2000); Lin and Atluri (2001); XueHong, ShengPing, and WenQuan (2007); Arefmanesh, Najafi, and Abdi (2008)]. Fig. 8 shows the average Nusselt number evaluated at the internal circle. The analytical Nusselt number for the pure diffusive case is also shown in Fig. 8. It is clear that the Nusselt number evaluated by the SEM, suddenly increases due to the onset of the natural convection. The analytical Nusselt number, based on the temperature distribution given by Eq. (19), has been evaluated as

$$Nu(t) = -\frac{d\Theta}{d\hat{R}} = -\frac{(1 - \eta_I)}{[(1 - \eta_I)\hat{R} + \eta_I]} \frac{1}{\ln(\eta_I)} \quad (20)$$

where  $\hat{R} = (r - r_i)/(r_m(t) - r_i)$ , and  $\eta_I = r_i/r_m(t)$ .

If we perform the heat balance at the interface ( $\hat{R}=1$ ), it is possible to evaluate the radial position of the melting front  $\eta_I(t)$  as a function of time in the conductive regime.

The equation governing the displacement of the interface is written as

$$\frac{d\eta_I^{-1}}{dt} = \frac{1}{\eta_I^{-1} St \ln(\eta_I^{-1})} \left( \frac{1 - \eta}{\eta} \right)^2 \quad (21)$$

Notice that in this equation the radius ratio  $\eta$  is present, because we have used the thermal time  $t_d$  to nondimensionalize the time derivative of the radial position of the melting front  $r_m(t)$ . After solving Eq. (21), we calculate the  $Nu$  number at the internal cylinder ( $\hat{R} = 0$ ) through the use of Eq. (20). It is shown that in the conductive regime, the Nusselt number evaluated by the SEM, is in agreement with the analytical solution. It is possible to observe that the onset of the convection is around  $t=0.34$ . Solving Eq. (21), at  $t=0.34$ , the value of  $\eta_I^{-1}=1.7$ , which corresponds to a radius ratio  $\eta_I=0.58$ . We have obtained a critical mode number  $m_c=7$ . According to the theory developed by Sahir et al. (1999), the critical azimuthal mode number for this radius ratio, without shear is around  $m_c=8$ , which is in qualitative agreement with the SEM results.

*4.2.2 Melting of an initially solid annular region with radius ratio  $\eta=0.35$ , and with shear ( $P = 0.02$ )*

Fig. 9 shows the isothermals at different times. Notice that as the melting process is carried out, the Rayleigh number  $Ra$ , the radius ratio  $\eta_I$  and the Reynolds number  $Re$  are time dependent. It is observed that due to the shear ( $\Omega^*=325.7$ ), the onset of the natural convection is delayed. In the previous case the onset appeared around  $t=0.34$  (see Figs. 7 and 8), whereas with shear the onset appears around  $t=0.44$ . Solving Eq. (21), at  $t=0.44$ , the value of  $\eta_I^{-1}=1.79$ , which corresponds to a radius

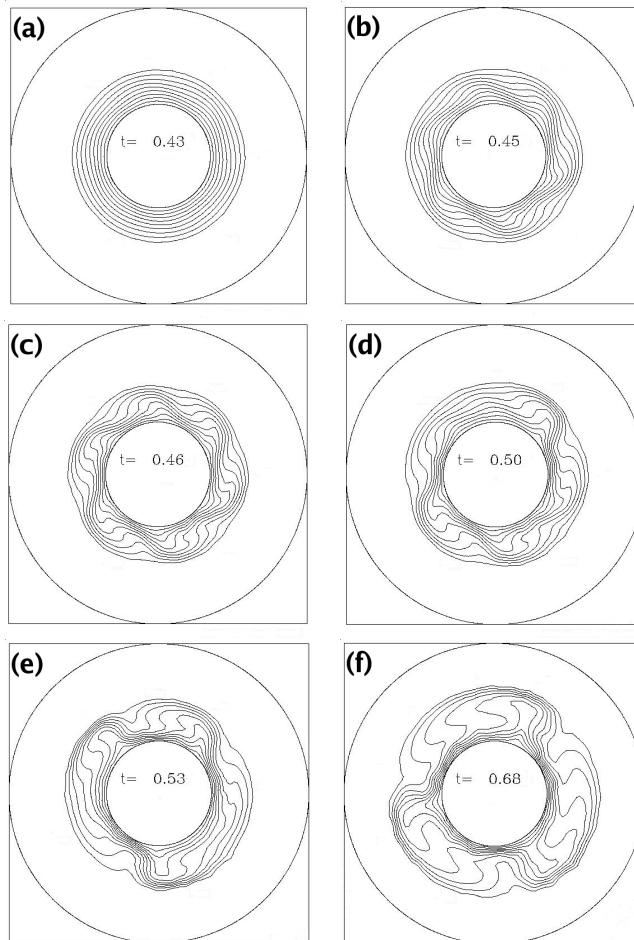


Figure 9: Non-steady natural convection in a concentric annulus with melting  $St=3.9$ . Isothermal lines, the temperature increment between isotherms is  $\Delta\Theta=0.1$ . Traveling pattern in a supercritical regime. Nondimensional period  $P=0.02$ .  $Ra$ ,  $\eta_I$ ,  $Re$  and  $m$  parameters are time dependent parameters.

ratio  $\eta_I=0.55$  and to a Reynolds number  $Re=5.7$ . Fig. 9 (b), shows that the critical mode number (around  $m_c=6$ ) is less than the case with no shearing ( $Re=0$ ), which is also in agreement with Sahir et al. (1999). However as the size of the liquid layer increases ( $Re$  number also increases) the mode number decreases. Zahir et al. (1999) have reported that in 2D electroconvection, the critical wavenumber is a monotonically decreasing function of the shear Reynolds number. The Nusselt

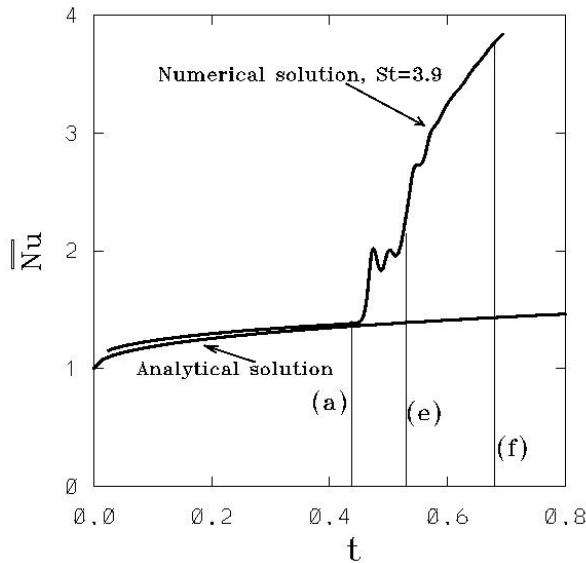


Figure 10: Average Nusselt number at the internal circle. With melting process,  $St=3.9$  and shearing  $\Omega^*=325.7$  ( $P=0.02$ ).  $Ra$ ,  $\eta_I$ ,  $Re$  and  $m$  parameters are time dependent. Analytical solution Eq. (20).

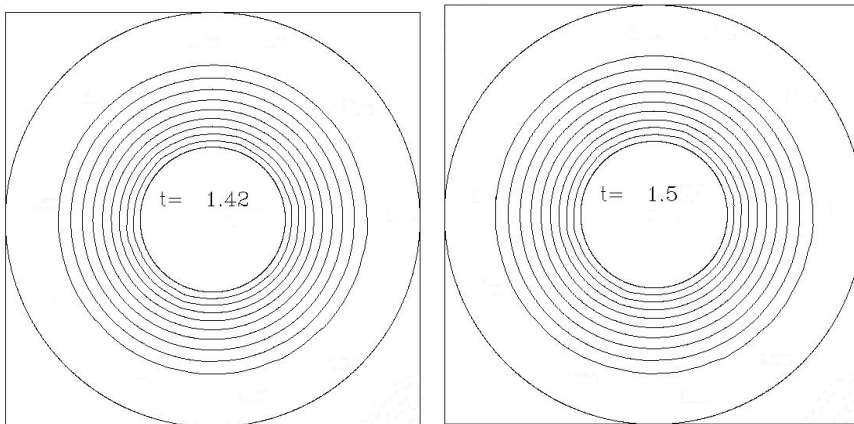


Figure 11: Isothermal lines in a concentric annulus with melting  $St=3.9$  and shearing for two cases: Left:  $\Omega^*=1628.6$  ( $P=0.004$ ) and Right:  $\Omega^*=3257.2$  ( $P=0.002$ ). The temperature increment between isotherms is  $\Delta\Theta=0.1$ . The shearing damps the natural convection.  $Ra$ ,  $\eta_I$  and  $Re$  parameters are time dependent.

number behaviour is shown in Fig. 10, it is seen that the convective pattern modification leads to a complex behaviour of the Nusselt number. In Fig. 10, the letters (a), (e) and (f), correspond to the patterns shown in Fig. 9.

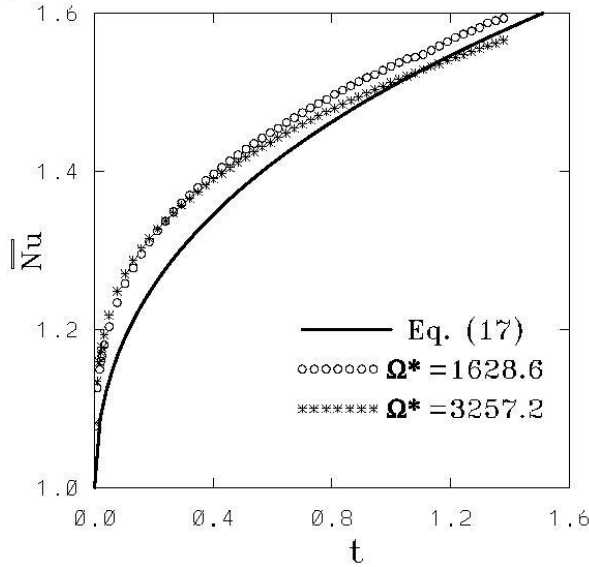


Figure 12: Average Nusselt number at the internal circle. With melting process,  $St=3.9$  and shearing for two cases:  $\Omega^*=1628.6$  ( $P=0.004$ ) and  $\Omega^*=3257.2$  ( $P=0.002$ ). The shearing damps the natural convection.  $Ra$ ,  $\eta_I$  and  $Re$  parameters are time dependent. Analytical solution Eq. (20).

It is observed an irregular behaviour in the vicinity of the (e) point. We see that as the mode number decreases (by the increase of the fluid layer), the mixed convection (traveling pattern and natural convection) of the large scale patterns, induces a much higher heat transfer rate (see point (f)). It is seen in Fig. 9 that the traveling pattern modifies the morphology of the interface, leading to an almost concentric position of the moving boundary. Hence the deformation of the interface is not as severe as it was in the case with no shearing (see Fig. 7).

#### 4.2.3 Melting of an initially solid annular region with radius ratio $\eta=0.35$ , and with shear ( $P=0.004$ and $P=0.002$ )

In order to estimate the influence of higher values of shearing on the convective onset, the heat transfer rate and the shape of the interface, we increased the value of the rotation rate at  $\Omega^*=1628.6$  ( $P=0.004$ ) and  $\Omega^*=3257.2$  ( $P=0.002$ ). We found

that in both cases the melting process was an almost pure diffusive phase change process.

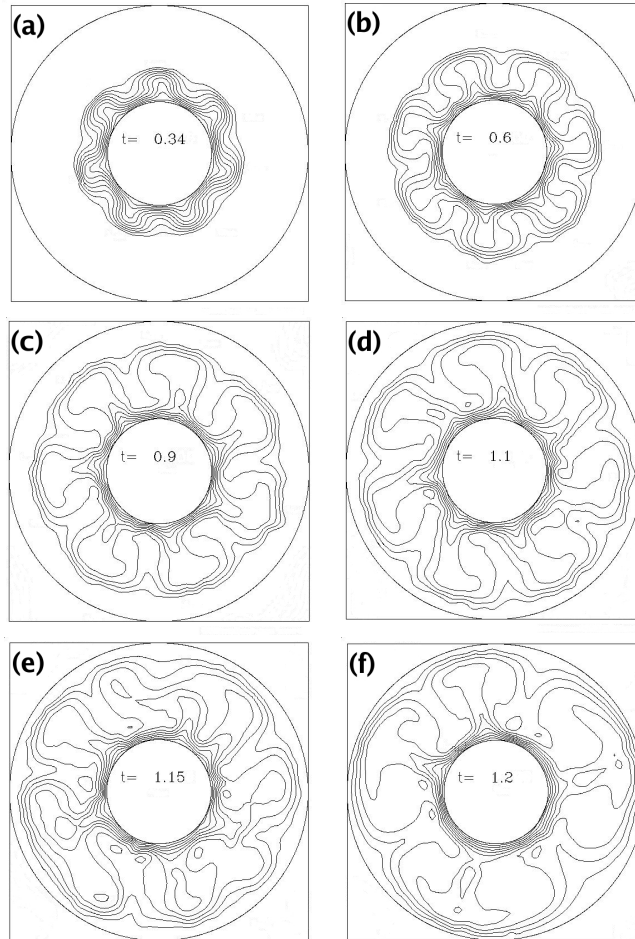


Figure 13: Non-steady natural convection in a concentric annulus with melting  $St=3.9$ . Isothermal lines, the temperature increment between isotherms is  $\Delta\Theta=0.1$ . Traveling pattern in a supercritical regime. Nondimensional period  $P=0.095$ .  $Ra$ ,  $\eta_I$ ,  $Re$  and  $m$  are time dependent parameters.

Fig. 11 shows the isothermal lines for both cases. It is seen that even for dimensionless times  $t=1.42$  (for the case with  $P=0.004$ ) and  $t=1.5$  (for the case with  $P=0.002$ ), the isotherms are concentric circles, hence there is no convective mode in the melting process.

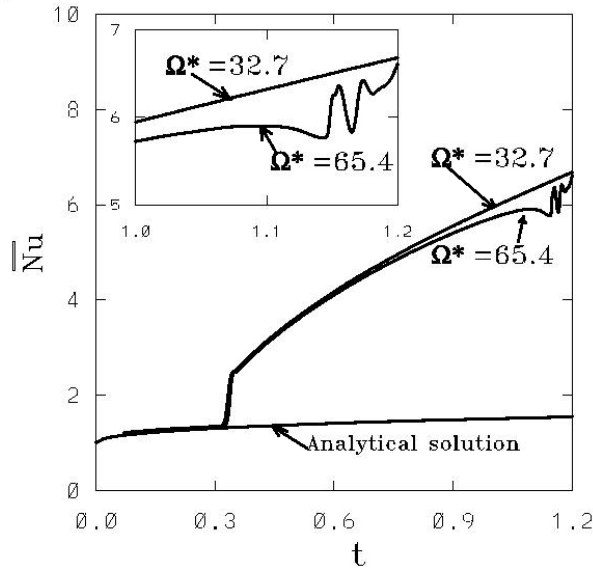


Figure 14: Average Nusselt number at the internal circle. With melting process,  $St=3.9$  and shearing for two cases:  $\Omega^*=32.7$  ( $P=0.19$ ) and  $\Omega^*=65.4$  ( $P=0.095$ ).  $Ra$ ,  $\eta$ ,  $Re$  and  $m$  parameters are time dependent. Analytical solution Eq. (20).

It is also observed that in both cases, the shape of the interface is a concentric circle, hence the shearing damps the convective cells and the shape of the interface remains smooth. Fig. 12 shows the average Nusselt number evaluated at the internal circle for the cases with  $P=0.004$  and with  $P=0.002$ . The analytical solution for the pure diffusive case, Eq. (20), is also shown. Notice that due to the damping of the convective onset, the average Nusselt number is very low as compared with the case with convective onset (see Fig. 10). It is seen that the  $\overline{Nu}$  number for the case with a lower rotation rate  $P=0.004$ , is higher than the case with higher angular speed  $P=0.002$ . Even though the isothermal lines are almost concentric circles, it is possible to observe (for the case with  $P=0.004$ ), small amplitude perturbations of the average Nusselt number, this is observed at around  $t=1.1$ . Nevertheless the heat transfer process is dominated by a diffusive mechanism.

#### 4.2.4 Melting of an initially solid annular region with radius ratio $\eta=0.35$ , and with shear ( $P=0.095$ and $P=0.19$ )

In the previous section it was shown that as the angular speed of the inner circle is increased to values  $\Omega^*=1628.6$  and  $\Omega^*=3257.2$ , the onset of the natural convection does not appear. It was also shown in section 4.2.2 that at an angular speed

$\Omega^*=325.7$ , the mode number of the convective cells is small even though the aspect ratio  $\eta_l=r_i/r_m(t)$  is high, hence it can be mentioned that the shearing dominates the convective cells, see Fig. 9. In this section it was decided to reduce the angular speed in order to investigate the influence of shear on a system where natural convection is dominant. Two new cases are presented with values of the angular speed of the inner circle at  $\Omega^*=32.7$  and  $\Omega^*=65.4$ . The results shown in Figs. 13 and 14 confirm the fact that low angular speeds allow the onset of the natural convection and pattern formation. Fig. 13 shows the time evolution of the melting process. Fig. 13 (a) shows that the convective onset occurs (for both cases) at around  $t=0.34$  (see also Fig. 14) with mode number  $m_c=7$ . Then the onset occurs earlier than the case with shearing with  $P=0.02$  ( $\Omega^*=325.7$ ), see section 4.2.2, but at the same time as the case without shearing, see section 4.2.1. Hence at angular speeds of the inner circle ( $\Omega^*=32.7$  and  $\Omega^*=65.4$ ), the Rayleigh-Bénard convection dominates the damping effect of the shear. The critical mode number for both cases is  $m_c=7$ . As time elapses for the case with  $\Omega^*=32.7$ , the traveling pattern remains with a mode number  $m=7$ , until the whole annular region is liquid (at  $t=1.2$ ). Fig. 14 shows that the Nusselt number for the case with  $\Omega^*=32.7$  shows a smooth monotonic increase, which means that there is no a significant change of the traveling flow pattern along the melting process (constant mode number  $m=7$ ). However for the case with  $\Omega^*=65.4$ , it is possible to observe that the flow pattern mode number changes from  $m_c=7$  to  $m_c=4$ . The change in the mode number begins at times larger than  $t=1$ , where a decrease in the heat transfer rate is apparent. Notice that at time around  $t=1.1$ , there is an irregular behaviour of the average Nusselt number and a modification of the flow pattern. It is possible to observe that the change of flow pattern occurs when almost the annular region is a fluid. It is interesting to mention that even though the natural convection is dominant, the shear leads to a smooth evolution of the interface, hence the remeshing process is not necessary as was the case shown in section 4.2.1. Regarding the heat transfer rate evaluated at the inner circle, it can be mentioned that as shearing is increased the Nusselt number is decreased.

## 5 Conclusions

The Spectral Element Method has been used to calculate the natural convection of a fluid (water) confined in a 2D circular annulus. The natural convection is driven by a radial gravity field (self gravity). This simplified model may be applied to calculate the thermal motion of the atmospheric wind at the terrestrial equatorial plane. The numerical calculations without melting and with shearing, have been successfully compared in a qualitative manner, with theoretical results and experimental data obtained in a problem which has an electrical instability source. With

no shearing we have found that there is no mean flow along the azimuthal direction. The results confirm the fact that shearing has a stabilizing effect on thermal convection, and that the most unstable mode travels in the direction of the rotation of the inner circle. It has been found that increasing the  $Re$  number, the net effect is a reduction of the azimuthal mode number. The obtained numerical results for the cases with melting and shear, have shown that as the melting process takes place, the  $Re$  number increases, leading to a decrease of the azimuthal wavenumber. It is shown that the traveling mode has an important effect on the shape of the interface. It seems that the traveling mode transports heat from the inner circle to the interface in a more uniform manner, consequently the annular fluid layer grows smoothly without severe deformation of the moving boundary, hence no remeshing is required. It has been found that as the angular speed is increased a reduction of the average Nusselt number evaluated at the inner circle is apparent. According to the results obtained in this research, it is possible to mention that: (i) a Couette shear flow may control the intensity and number of convective plumes in the fluid layer, hence the transport of impurities towards the interface is diminished, and (ii) a Couette shear flow may control the shape of the moving interface, then the imperfections of the interface (which may lead to the generation of residual stresses in the solid material) are diminished. The numerical simulations in the non-linear regime with melting and shear constitute an important source of information about the different bifurcations that appear in a dynamical system where the governing parameters (Rayleigh number  $Ra$ , radius ratio  $\eta_I$  and Reynolds number  $Re$ ) are continuously changing. This information may also be useful to verify linear and non-linear stability theories.

**Acknowledgement:** Financial support for this investigation was provided by DGAPA-UNAM (PAPIIT project IN102506-3) and DGSCA-UNAM through the Visualization Observatory (Ixtli project). Most of the computations were carried out in the supercomputers of DGSCA-UNAM.

## References

**Arefmanesh, A.; Najafi, M.; Abdi, H.** (2008): Meshless Local Petrov-Galerkin Method with unity test function for non-isothermal fluid flow. *CMES: Computer Modeling in Engineering & Sciences*, vol. 25, pp. 9–22.

**Deyirmenjian, V. B.; Zahir, A. D.; Morris, S. W.** (2005): Codimension-two points in annular electroconvection as a function of aspect ratio. *Physical Review E*, vol. 72, pp. 036211.

**Inaba, H.; Fukuda, T.** (1984): An experimental study of natural convection in an inclined rectangular cavity filled with water at its density extremum. *J. Heat Transfer*, vol. 106, pp. 109–115.

**Karniadakis, G. E.; Sherwin, S. J.** (1999): *Spectral/hp Element Methods for CFD*. Oxford University Press.

**Langford, W. T.; Rusu, D. D.** (1998): Pattern formation in annular convection. *Physica A*, vol. 261, pp. 188–203.

**Lin, H.; Atluri, S. N.** (2000): The meshless local petrov-galerkin (mlpg) method for convection-diffusion problems. *CMES: Computer Modeling in Engineering & Sciences*, vol. 1, pp. 45–60.

**Lin, H.; Atluri, S. N.** (2001): The meshless local petrov-galerkin (mlpg) method for solving incompressible navier-stokes equations. *CMES: Computer Modeling in Engineering & Sciences*, vol. 2, pp. 117–142.

**Mai-Cao, L.; Tran-Cong, T.** (2008): A meshless approach to capturing moving interfaces in passive transport problems. *CMES: Computer Modeling in Engineering & Sciences*, vol. 31, pp. 157–188.

**Mai-Duy, N.; Mai-Cao, L.; Tran-Cong, T.** (2007): Computation of transient viscous flows using indirect radial basis function networks. *CMES: Computer Modeling in Engineering & Sciences*, vol. 18, pp. 59–77.

**Net, M.; Alonso, A.; Sánchez, J.** (2003): From stationary to complex time-dependent flows at moderate Rayleigh numbers in two-dimensional annular thermal convection. *Physics of Fluids*, vol. 15, pp. 1314–1326.

**Patera, A. T.** (1984): A spectral element method for fluid dynamics: laminar flow in a channel expansion. *Journal of Computational Physics*, vol. 54, pp. 468–488.

**Rønquist, E. M.** (1988): *Optimal Spectral Element Methods for the unsteady three-dimensional incompressible Navier-Stokes equations*. Phd Thesis, Massachusetts Institute of Technology.

**Rønquist, E. M.; Patera, A. T.** (1987): A Legendre Spectral Element Method for the Stefan Problem. *International Journal for Numerical Methods in Engineering*, vol. 24, pp. 2273–2299.

**Tsai, P.; Zahir, A. D.; Deyirmenjian, V. B.; Morris, S. W.** (2007): Direct numerical simulation of supercritical annular electroconvection. *Physical Review E*, vol. 76, pp. 026305.

**Tsuda, T.; Murayama, Y.; Wiryosumarto, H.; Harijono, S. W. B.; Kato, S.** (1994): Radiosonde observations of equatorial atmosphere dynamics over Indonesia: 1 Equatorial waves and diurnal tides. *Geophysical Research*, vol. 99, pp. 491–505.

**Tsuda, T.; Murayama, Y.; Wiryosumarto, H.; Harijono, S. W. B.; Kato, S.** (1994): Radiosonde observations of equatorial atmosphere dynamics over Indonesia: 2 Characteristics of gravity waves. *Geophysical Research*, vol. 99, pp. 507–516.

**XueHong, W.; ShengPing, S.; WenQuan, T.** (2007): Meshless Local Petrov-Galerkin Collocation Method for two-dimensional heat conduction problems. *CMES: Computer Modeling in Engineering & Sciences*, vol. 22, pp. 65–76.

**Zahir, A. D.; Deyirmenjian, V. B.; Morris, S. W.** (1999): Electrically driven convection in a thin annular film undergoing circular Couette flow. *Phys. Fluids*, vol. 11, pp. 3613–3628.

**Zahir, A. D.; Deyirmenjian, V. B.; Morris, S. W.** (2001): Bifurcations in annular electroconvection with an imposed shear. *Physical Review E*, vol. 64, pp. 036212.

**Zahir, A. D.; Deyirmenjian, V. B.; Morris, S. W.; Bruyn, J. R. D.** (1998): Annular electroconvection with shear. *Phys. Rev. Lett.*, vol. 80, pp. 964–967.